Theor Chem Acc (2002) 107:272–281
DOI 10.1007/s00214-002-0330-5

Theoretical Chemistry Accounts

Regular article

Band structure representations of the electronic structure of one-dimensional materials with helical symmetry

Wingfield V. Glassey[1], **Roald Hoffmann**[2]

[1] Department of Chemistry, The College of Wooster, 943 College Mall, Wooster, OH 44691-2363, USA
[2] Department of Chemistry and Chemical Biology, Cornell University, Ithaca, NY 14853-1301, USA

Received: 5 November 2001 / Accepted: 14 January 2002 / Published online: 3 May 2002

Abstract. The relationship between band structure and the topology of the orbital interactions between neighboring chemical units comprising several model one-dimensional polymers with helical (screw-axis) symmetry is analyzed. A perturbative model of orbital interactions based on a tight binding implementation of the extended Hückel method is developed. The model accounts for both the band topologies and the seemingly anomalous band extrema within the Brillouin zone constructed using the chemical repeat unit of the polymer.

Key words: Band structure – One-dimensional – Polymer – Helix

1 Introduction

There are some polymers in which helical (screw-axis) symmetry is apparent. An example is *trans*-polyacetylene (Scheme 1, **1**), or the hypothetical chain of H_2 molecules (Scheme 2, **2**) (a pedagogical example).

1

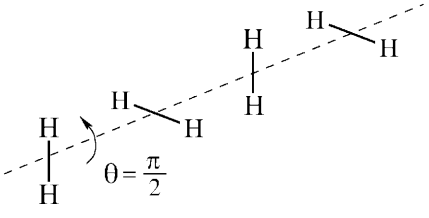

2

The chemical repeat unit in **1** is CH, in **2** H_2. In each case the translational repeat unit is obtained by doubling the chemical repeat unit, ie. the translational repeat unit contains two chemical units – 2 CH for **1** and 2 H_2 in the case of **2**. The primary motivation for our work is a systematic exposition of the relationship between the band structures of helical polymers and the topologies of the orbital interactions between the chemical building blocks of the polymers.

In the absence of level crossings, the band extrema for one-dimensional polymers, by which we mean materials with one-dimensional periodic potentials, i.e.

$$V(z) = V(z + a) \ ,$$

where a is the translational period, always occur at either the center or the edges of the Brillouin zone (BZ). In contrast we note that this is not the case if we construct the band structure for the H_4 stack (Scheme 3, **3**), (another pedagogical example) using the chemical repeat unit.

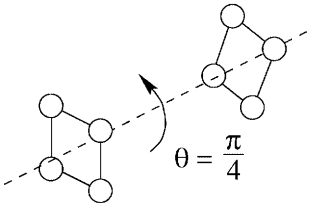

3

The band structure for **3** is shown in Fig. 1. The occurence of extrema, such as those for bands I and II in Fig. 1, that do not coincide with either the center or the edges of the BZ for polymers with helical symmetry is the second factor motivating our study of these systems. As noted previously by Bozovic [1], such extrema may arise in quasi-one-dimensional polymers constructed by combining chemical units that are themselves either two- or three-dimensional. The electron potential associated with quasi-one-dimensional polymers is, in general, not one-dimensional; however, it is periodic in one dimension i.e.

$$V(x, y, z) = V(x, y, z + a) \ ,$$

where a is once more the translational repeat distance.

In the course of this study we develop a mathematical formalism capable of accounting for the existence and position of such extrema within the BZ. In order to

Correspondence to: W.V. Glassey
e-mail: wglassey@wooster.edu

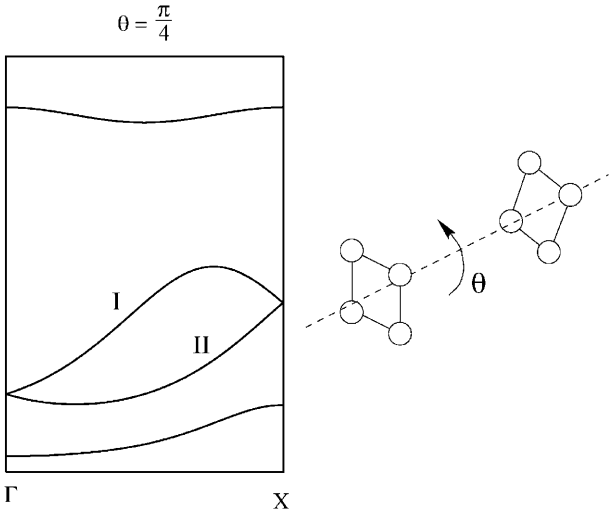

Fig. 1. The band structure for an H_4 stack generated by the repeated application of screw-axis symmetry with an associated 45° rotation

maintain a focus on the relation between band structure and the topology of the orbital interactions between neighboring chemical units in a polymer, we chose to construct our models using only hydrogen. By doing so we avoid any complications arising from the symmetry properties of individual atomic basis orbitals. The band structure calculations were performed using a tight binding scheme within a one-electron extended Hückel formalism [2]. The details of the calculations are given in the Appendix.

2 Introducing translation–rotation symmetry

We begin our discussion by considering the one-dimensional lattice with translational period, a shown in Scheme 4.

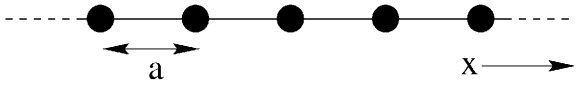

4

The wavefunctions for this lattice have the "Bloch form",

$$\phi_i(x,k) = \sum_n \mathbf{T}^n U_i(x) \mathrm{e}^{inka} \quad , \tag{1}$$

on defining the translation operator, $\mathbf{T}^n$, by the relation

$$\mathbf{T}^n U_i(x) \equiv U_i(x+na) \quad . \tag{2}$$

In what follows the basis $\{U_i\}$ is the set of molecular orbitals (MOs) contained within the unit cell. Consider the band structure resulting from a side-on stacking of hydrogen molecules as illustrated in Fig. 2. For this case the basis $\{U_i\}$ consists of the bonding (σ) and anti-bonding (σ^*) molecular orbitals of a single hydrogen molecule – the basic translational unit of the system.

The H_2 stack is the simplest example of a one-dimensional polymer which can be constructed by the application of either pure translational symmetry or translation–rotation symmetry. If we now generate the H_2 stack using translation–rotation (screw-axis) symmetry, we obtain the band structure shown in Fig. 3.

Clearly the band structures for the H_2 stack shown in Figs. 2 and 3 are different. In order to understand these differences we must develop a mathematical formalism to describe the wavefunctions of the H_2 stack generated using a translation–rotation operator, $\mathbf{S}_\alpha^\tau$. The operation $\mathbf{S}_\alpha^\tau$ corresponds to a translation by τ, followed by a rotation, α, about the translation axis. Scheme 5 illustrates the one-dimensional stack of diatomics resulting from the application of the operator $\mathbf{S}_{\frac{\pi}{2}}^\tau$ i.e. a fourfold screw axis, to a heteronuclear diatomic molecule. The rotation is arbitrarily defined to be counterclockwise.

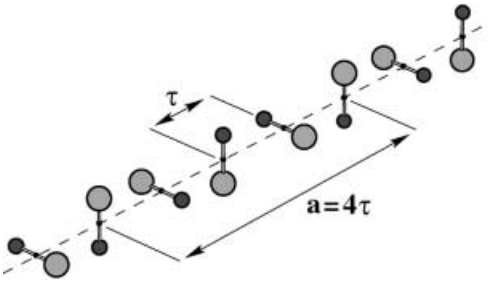

5

By analogy with Eq. (1) the set of symmetry-allowed wavefunctions for a system with translation-rotation symmetry has the general form

$$\phi_i(x,k') = \sum_m (\mathbf{S}_\alpha^\tau)^m U_i(x) \mathrm{e}^{imk'a} \quad , \tag{3}$$

where, by analogy with the translational symmetry case, we have defined a wavevector, k'. We must now examine the relation between k for the translational case and k' for the translation–rotation case.

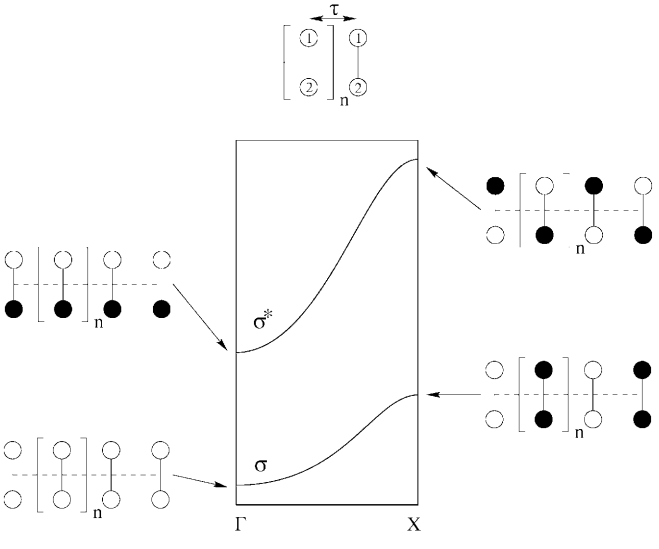

Fig. 2. Band structure for a 1D chain of H_2 units stacked side-on

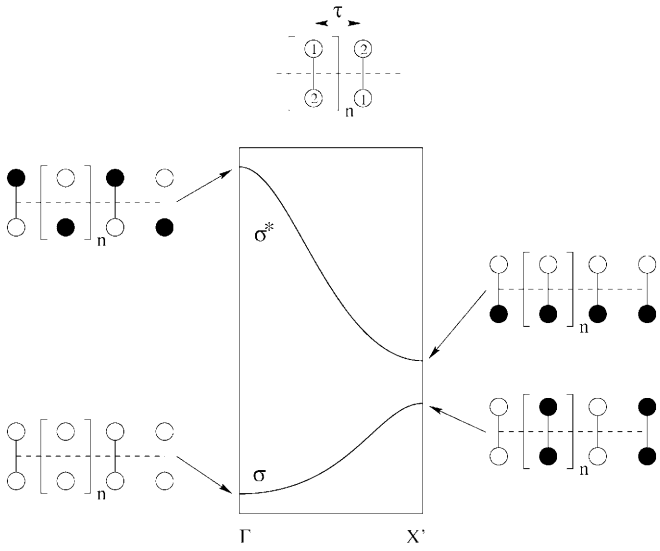

Fig. 3. Band structure for a 1D chain of H_2 units stacked side-on. The chain is generated using the translation–rotation symmetry operator S_{π}^{τ}

From Scheme 5 we note that if we apply $\mathbf{S}_{\pi}^{\tau}$ four times we end up with an operation equivalent to a single application of the operator **T**, as defined by Eq. (2). In general, we may proceed to connect the operators **S** and **T** through a relation of the form

$$(\mathbf{S}_{\alpha}^{\tau})^{v} \equiv \mathbf{T} \ , \tag{4}$$

where $v = \frac{2\pi}{\alpha}$ is the number of translation–rotation operations required to generate a full turn of the helix.

Using Eq. (4) we can write Eq. (1) in the form

$$\phi_i(x,k) = \sum_n (\mathbf{S}_{\alpha}^{\tau})^{nv} U_i(x) \mathrm{e}^{inka} \ . \tag{5}$$

Thus if Eqs. (3) and (5) are to be equivalent for a complete turn of the helix, as defined by Eq. (4), we must have $mv = n$. Hence, the wavevectors k and k' are related by the expression

$$k' = vk = \left(\frac{a}{\tau}\right)k \ . \tag{6}$$

Equation (6) implies that the size of the BZ for translation–rotation symmetry, which is defined as the interval $-\frac{\pi}{\tau} < k' \leq \frac{\pi}{\tau}$, scales linearly with the number of translation–rotation operations, v, required to complete a full turn of the helix [3]. By convention the BZ for the case of translation–rotation symmetry is known as the Jones zone (JZ) [4]. Consider, for example, the helix in Scheme 5 (**5**) for which $v = 4$. The JZ for **5** is thus, by 6, 4 times larger than the BZ for the purely translational case defined by the translational cell a.

Now that we have some understanding of how to map between the BZ and the JZ representations of the band structure let us now return to the case of the H_2 stack discussed previously. On examination of the translational and translation–rotation band structures shown in Figs. 2 and 3, respectively, it is immediately apparent that the BZ and JZ representations of the H_2 stack are different. Indeed the antibonding (σ^*) band "runs up" from Γ ($k = 0$) to X ($k = \frac{\pi}{a}$) in the case of translational symmetry and "runs down" from Γ ($k' = 0$) to X' ($k' = \frac{\pi}{\tau} = \frac{\pi}{a}$) for translation–rotation symmetry.

We can understand this difference if we consider the iconic band representations given in Figs. 2 and 3, where we have used shaded and unshaded spheres to represent H(1s) orbitals of opposite phase. The σ^* band is antisymmetric with respect to inversion about the center of the H–H bond. Thus, for the case of translational symmetry the σ^* band becomes increasingly antibonding between H_2 units in the stack on going from Γ to X. The reverse is true for the σ^* band in the JZ representation.

In contrast, the σ band – which is invariant with respect to inversion about the H–H bond center – behaves in an identical manner in both the BZ and the JZ representations.

We have seen this kind of behavior before [5]. The π bonding and antibonding bands in planar all-trans polyisocyanide (Scheme 6, **6**) run up on constructing the BZ from a translational repeat unit consisting of a single isocyanide. In contrast, the application of screw-axis symmetry to a single isocyanide results in π bonding and antibonding bands that run down from the center of the BZ.

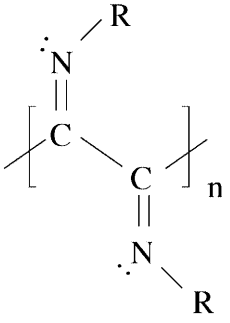

6

In the following discussions we investigate the similarities and differences in band topology for JZ and BZ representations of the electronic structure of several model one-dimensional polymers and seek to understand the conditions under which the JZ and BZ representations are equivalent.

3 Investigating band topology for translation–rotation symmetry

At this point in the discussion it proves useful to investigate the band topologies in both the BZ and the JZ representations for several simple one-dimensional polymers closely related to the H_2 stack discussed previously. From this point in the discussions we make use of the relation $E(k) = E(-k)$ and focus our attention on the "irreducible" part of the BZ and JZ defined by the intervals $[\Gamma, X]$ and $[\Gamma, X']$ respectively.

We begin by again considering the band structure of the H_2 stack, this time using a translational cell containing not one but two H_2 units. We note that the BZ for the "doubled cell" is only half the width of that for the single cell shown in Fig. 2 and is denoted by the interval Γ to $X''(=\frac{X}{2})$.

On remembering that the BZ representation is periodic with a period equal to the width of the complete BZ, i.e. $\frac{2\pi}{a}$, where a is the translational unit cell length, we can check to see if the band structure for the double cell "unfolds" to that for the case of a single H_2 molecule per translational cell (Fig. 2). The extended zone or "unfolded" band structure for the doubled translational cell is shown in Fig. 4.

The bonding and antibonding bands for the translational cell shown in Fig. 2 can be identified amongst the bands for the doubled cell shown in Fig. 4 on tracing out monotonically increasing bands on the interval $[0, 2X'']$ beginning at the points f and c respectively.

Indeed we can trace out these bands by translating sections of the band structure contained within the BZ ($-X'' < k \leq X''$) by $2X'' \equiv \frac{\pi}{a}$. Thus, we are able to unfold the band structure for the doubled translational cell to reproduce the band structure for the simple translational cell and we conclude that they are in fact equivalent representations of the electronic structure of the H_2 stack as they must be.

Further, the σ^* band for the case of S_π^a symmetry (Fig. 3) can be identified as the monotonically decreasing band running down from point a in Fig. 4 on the interval Γ to $2X''$. Once more the bands for the JZ representation can be generated by translating elements of the band structure for the doubled translational cell lying in the BZ. Thus, we conclude that the JZ representation based on a single translational unit and the BZ representation for a doubled translational cell are equivalent.

Hence, it appears that in order to be consistent with both translational and translation–rotation descriptions of the H_2 stack based on a unit cell containing a single H_2 unit, we should adopt the doubled translational cell as our model. Before moving on it is useful to remember that the doubled translational cell is equivalent to one complete turn of the helix defined by the operator S_π^a – albeit a "paper helix" in the present case.

We return to this conclusion later in the discussion after we have had a chance to investigate the JZ and BZ representations of the band structure for the one-dimensional polymer resulting from a 90° rotation of alternate H_2 units in the H_2 stack considered thusfar. The "alternating stack" **7** represents the next level of sophistication in our discussion as it extends into both spatial dimensions orthogonal to the translational axis.

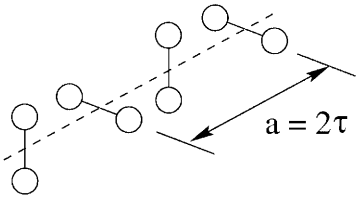

7

We begin by considering the band structure for both JZ and BZ representations of **7**. The representations are based on translation–rotation and pure translational cell lengths of τ and $a = 2\tau$, respectively, and are shown in Fig. 5. The BZ representation of **7** is shown for both the first and second BZs ([Γ, X] and (X,2X], respectively) to illustrate how the σ band unfolds to reproduce the σ band for the JZ representation [$\Gamma \rightarrow X'(=2X)$].

On turning our attention to the doubly degenerate σ^* band, we note a discrepency between the BZ and JZ representations. For the case of pure translational symmetry we observe a monotonically increasing σ^* band "running up" from the Γ point, and for the case of translation–rotation symmetry we observe that the σ^* band runs down from Γ towards the zone edge.

We can reconcile this difference if we adopt the conclusion made previously for the case of the nonalternate H_2 stack. On considering the BZ representation of the band structure for the "doubled" translational cell ($a = 4\tau$) shown in Fig. 6 we can identify both the σ and σ^* bands from the JZ representation. Further, we can

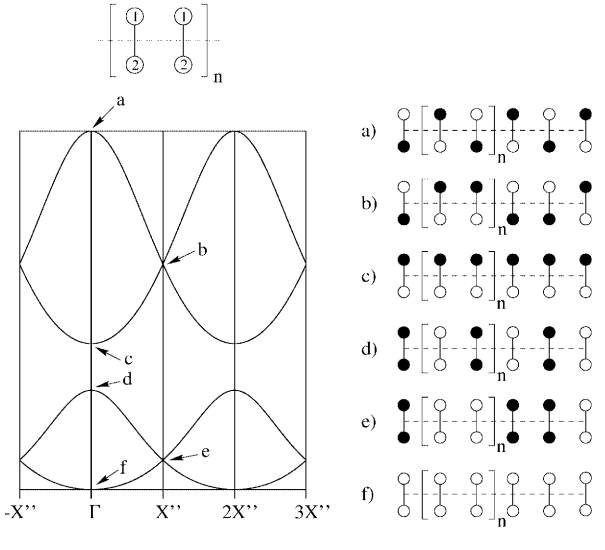

Fig. 4. Band structure for the $^1_\infty[(H_2)_2]$ chain in the extended Brillouin zone (BZ) representation

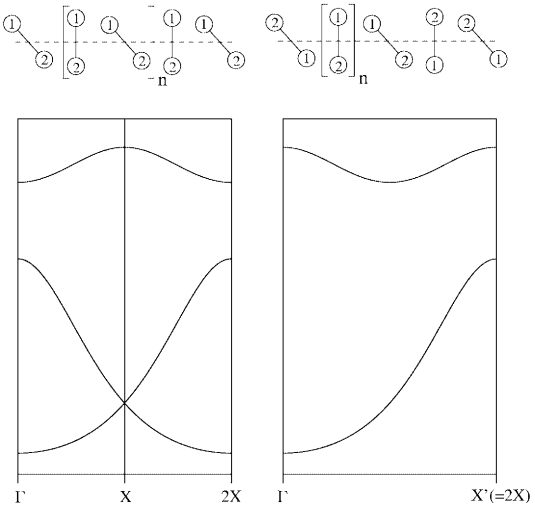

Fig. 5. Band structure representations of the electronic structure of the alternating H_2 stack constructed from, on the *left*, a translational unit cell comprising two H_2 units and on the *right*, a single H_2 unit subject to translation–rotation symmetry

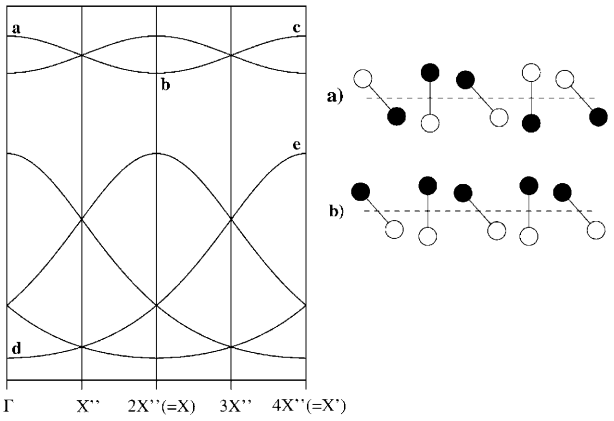

Fig. 6. Band structure for the alternating H_2 stack for a translational cell consisting of four H_2 units

also identify the second, monotonically decreasing, σ band for the purely translational case in Fig. 5.

The σ band in the JZ representation, a band running up from the Γ point to the zone edge at $X' = 4X$, can be easily identified as a band running between the points d and e in Fig. 6. The σ^* band – which traces the path a → b → c – exemplifies a quite different type of band topology by ''oscillating'' between extrema whose energy separation is determined by the strength of the orbital interactions between hydrogen atoms on alternate H_2 units in the stack. This is best illustrated by considering the iconic representations of the bands at points a and b shown in Fig. 6.

Thus, once more, it appears that in order to provide a consistent representation of the electronic structure of a material with translation–rotation symmetry using only translational symmetry it is necessary to consider a translational unit cell length equivalent to one complete turn of the helix generated by the translation–rotation symmetry.

4 The second dimension: two-dimensional repeat units

We now progress to the next level of complexity – the relation between band topology and the symmetry of the basic structural unit of the polymer. We chose to study the electronic structure of polymers generated by stacking square planar H_4 units as illustrated in Scheme 8.

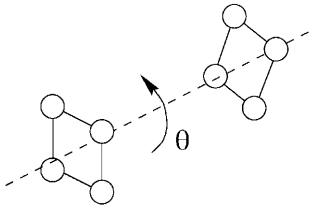

8

The stacking angle, θ, affords us the opportunity to study the band structure as a continuous function of θ for the transitions between pure translational symmetry ($\theta = \frac{n\pi}{2}; n = 0, 1, 2, 3$) and translation-rotation symmetry.

But why study the square-planar H_4 unit? Why not study the stacking of planar H_3 units or H_6 units? The answer to these questions is simply that the H_4 unit is the simplest structural unit that, by virtue of the symmetry it possesses, illustrates the various band topologies we have found to date for systems with translation–rotation symmetry. Consider the sequence of band structures shown in Fig. 7.

Each band structure corresponds to a particular value of the stacking angle as defined by Scheme 8. On going from left to right, the value of θ increases and we observe the emergence of several notable changes in the band structure. We begin our analysis on the left-hand side of Fig. 7 with the $\theta = 0$ case – an eclipsed stack of H_4 units. To understand the band structure we must first remind ourselves of the form of the MOs of the H_4 unit.

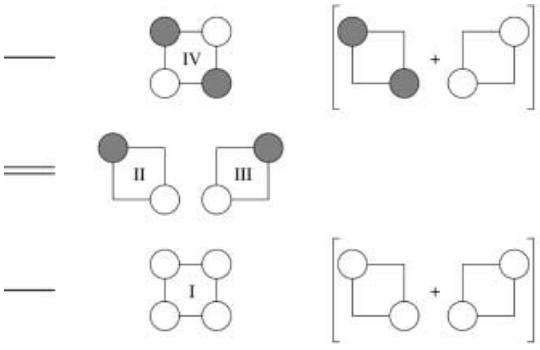

9

In Scheme 9 we have chosen to visualize the MOs of the square-planar H_4 unit in terms of contributions from two orthogonal H_2 fragments. The construction of an H_4 unit from two H_2 units enables us to draw direct parallels between the band structures for the H_4 and H_2 stacks. Proceding in this way we would expect that bands I and IV for the $\theta = 0$ case should have the same topology as the σ bands in the H_2 stacks since we are able to decompose MOs I and IV into contributions from the σ orbitals on each of the H_2 fragments. Indeed

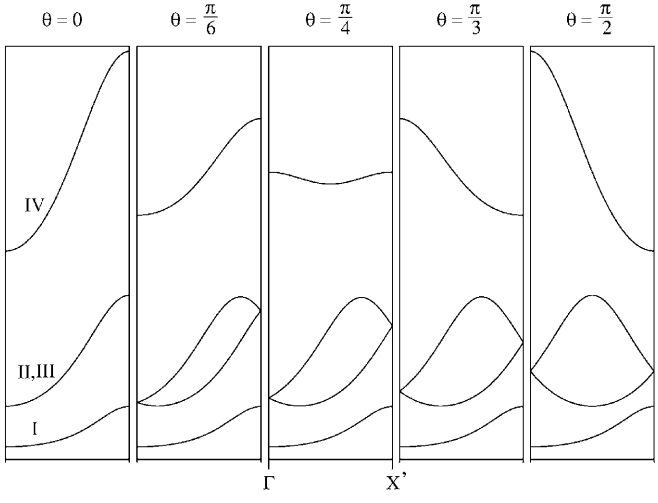

Fig. 7. Band structure for the H_4 stack in the Jones zone (*JZ*) representation as a function of the stacking angle, θ

bands I and IV run up from the Γ point and have the same shape as the σ band of the H_2 stack. Further, bands II and III, which are degenerate throughout the BZ for $\theta = 0$ on symmetry grounds, are analogous to the σ^* band shown in Fig. 2 for the purely translational case.

Next we consider the $\theta = \frac{\pi}{6}$ case and the transition from pure translational symmetry to translation–rotation symmetry. The most striking change in the band structure is the separation of the formerly degenerate bands II and III to form a "hysteresis-loop"-type band structure with band extrema that no longer coincide with the center and edges of the JZ. Previously we noted the existence of similar extrema in the band structures of one-dimensional carbon chains [6] – the backbone of many organic polymers. In the case of polyethylene, polyacetylene, and other polymers based on one-dimensional carbon chains, the occurence of band extrema that do not coincide with either the center or the edges of the BZ is the result of *s–p* mixing in the carbon skeleton. Clearly *s–p* mixing cannot be responsible for the extrema in Fig. 7.

For polymers such as the H_4 stack **8**, which possess translational symmetry and no level crossings, band extrema are found only at the center and edges of the BZ. Thus, we now focus our efforts on understanding why the band extrema no longer occur at the center and edges of the JZ for the case of translation–rotation symmetry.

In order to understand this behavior we must now formalize somewhat our hypothesis that the topology of bands II and III for the H_4 stack may be reproduced by considering the interaction of the σ^* bands of two interpenetrating H_2 stacks. Consider the generic H_2 stack **10** defined by the translation, τ, and the stacking angle, θ. If we combine two H_2 stacks of the form **10** by rotating one stack by 90° with respect to the other we arrive at the H_4 stack **11**. The atoms belonging to each H_2 chain in **11** are identified by the atom shading.

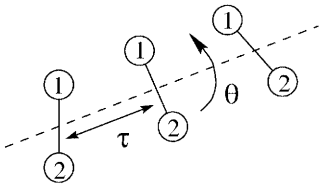

10

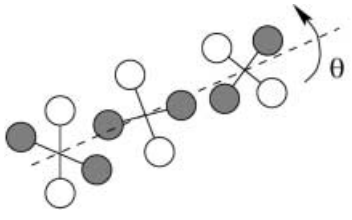

11

In order to evaluate the band structure derived from the σ^* bands of the interpenetrating H_2 stacks it is necessary to consider how the σ^* orbital of an H_2 unit interacts with the σ^* orbitals of neighboring H_2 units in both stacks. In what follows we consider only the interactions between the σ^* orbital of an H_2 fragment within an H_4 unit and the σ^* orbitals of the H_2 fragments in the nearest-neighbor H_4 unit. This is a sufficiently good approximation to allow us to develop a qualitative picture of how the stacking angle influences band topology.

We begin by writing an expression for the energy of the i^{th} band, $E_i(k,\theta)$, in the form

$$E_i(k,\theta) = E_i^{(0)}(\theta) + E_i^{(1)}(k,\theta) + \mathrm{E}_i^{(2)}(k,\theta) \ , \tag{7}$$

where the terms $E_i^{(0)}(\theta)$ ($i = 1, 2$) define the energies of the σ^* orbitals of the H_2 units abstracted from a single H_4 molecule **8**.

The θ-dependence of the zeroth-order terms, $\mathrm{E}_i^{(0)}(\theta)$, is most clearly understood in terms of a mixing of MOs II and III for the H_4 unit **9**. The lack of symmetry planes for the generic H_4 stack **11** affords the opportunity for a "remixing" of the σ^* orbitals on the H_2 fragments comprising a single H_4 unit of the stack. The orbital mixing within an H_4 unit is illustrated in Scheme 12.

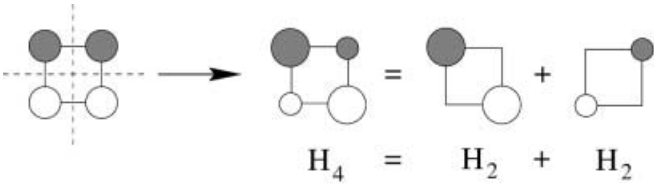

12

Thus, the degeneracy of the σ^* orbitals II and III for the case of pure translational symmetry is simply a special case of the more general nondegenerate case defined by $\theta \neq \frac{n\pi}{2}; n = 0, 1, 2, 3$.

On choosing to construct the band structure of the H_2 stack **7** by considering first the interaction between H_2 units in a simple H_2 stack [denoted by $E_i^{(1)}(k,\theta)$ in Eq. 7] and subsequently the interaction between interpenetrating H_2 stacks [$E_i^{(2)}(k,\theta)$ in Eq. 7] we may clearly identify the interactions responsible for the changes in band topology observed on varying the stacking angle in Fig. 7.

5 Tight binding models of band structure

We now introduce the tight binding formalism employed throughout this study [2] before developing expressions for the explicit θ- and k-dependence of the band energy $E_i(k,\theta)$ defined by Eq. (7). Within the tight binding formalism we seek a solution of the generalized eigenvalue equation

$$\hat{\mathbf{H}}(k,\theta)C_i(k,\theta) = E_i\hat{\mathbf{S}}(k,\theta)C_i(k,\theta) \ , \tag{8}$$

for each eigenstate, i, as a function of the wavevector, k, and the stacking angle, θ. The overlap and Hamiltonian matrices are defined by

$$\hat{\mathbf{S}}(k,\theta) = \sum_R \hat{\mathbf{S}}(R,\theta)\mathrm{e}^{ikR} \tag{9}$$

and

$$\hat{\mathbf{H}}(k,\theta) = \sum_R \hat{\mathbf{H}}(R,\theta)\mathrm{e}^{ikR} \ , \tag{10}$$

respectively. The index $R = n\tau; n = 0, 1, 2, \ldots$ serves to identify the individual H_4 units within polymer **11**.

On choosing to consider only nearest-neighbor interactions between H_4 units we may write Eqs. (9) and (10) in the forms

$$\hat{\mathbf{S}}(k,\theta) \approx \hat{\mathbf{S}}(0) + \hat{\mathbf{S}}(\tau,\theta)\mathrm{e}^{ik\tau} \tag{11}$$

and

$$\hat{\mathbf{H}}(k,\theta) \approx \hat{\mathbf{H}}(0) + \hat{\mathbf{H}}(\tau,\theta)\mathrm{e}^{ik\tau} \ , \tag{12}$$

The zeroth-order Hamiltonian and overlap matrices, $\hat{\mathbf{H}}(0)$ and $\hat{\mathbf{S}}(0)$, respectively, define the interaction between the two σ^* basis functions associated with a single H_4 unit of the stack and give rise to the zeroth-order energy term $E_i^{(0)}(\theta)$ in Eq. (7).

On choosing to construct the H_4 stack from two interpenetrating H_2 stacks, which can be in turn constructed from individual H_2 units, we may consider the perturbation of the molecular H_2 problem – as defined by the matrices $\hat{\mathbf{S}}(\tau,\theta)$ 11 and $\hat{\mathbf{H}}(\tau,\theta)$ 12 – to be the sum of two distinct perturbations. Consider the overlap matrix, $\hat{\mathbf{S}}(k,\theta)$, in Eq. (11). The perturbation applied to the molecular problem is written

$$\hat{\mathbf{S}}(\tau,\theta)\mathrm{e}^{ik\tau} = \sum_i S_{ii}(\tau,\theta)\mathrm{e}^{ik\tau} + \sum_{j\neq i} S_{ij}(\tau,\theta)\mathrm{e}^{ik\tau} \ , \tag{13}$$

where $i,j = \{1,2\}$.

The first term on the right-hand side of Eq. (13) describes the interaction between the σ^* orbitals of the H_2 units comprising a single H_4 unit of the H_4 stack **10** and their nearest neighbors in their respective H_2 stacks. In contrast, the second term on the right-hand side of Eq. (13) describes the interaction between the σ^* orbitals of the H_2 units in an H_4 unit and the σ^* orbitals of the H_2 units belonging to a different H_2 stack in the neighboring H_4 unit.

Thus, on constructing an expression analogous to Eq. (13) for the perturbation applied to the Hamiltonian $\hat{\mathbf{H}}(\tau,\theta)$ in Eq. (12) we can define the energy corrections $E^{(1)}$ and $E^{(2)}$ from Eq. (7) by the relations

$$E_i^{(1)}(k,\theta) = H_{ii}(\tau,\theta)\mathrm{e}^{ik\tau} \quad (i=1,2) \ , \tag{14}$$

$$E_1^{(2)}(k,\theta) = \frac{|H_{12}(\tau,\theta)\mathrm{e}^{ik\tau}|^2}{\Delta E^{(0)}(\theta)} \ , \tag{15}$$

and

$$E_2^{(2)}(k,\theta) = -\frac{|H_{21}(\tau,\theta)\mathrm{e}^{ik\tau}|^2}{\Delta E^{(0)}(\theta)} \ . \tag{16}$$

In Eqs. (14), (15), and (16) we extracted the explicit k-dependence of the band energies. We now turn our attention to determining the explicit θ-dependence of the matrix elements $H_{ij}(\tau,\theta)$, and begin by considering the θ-dependence of the corresponding overlap matrix elements, $S_{ij}(\tau,\theta)$.

Consider the overlap between the σ^* orbitals on neighboring H_2 units of the H_2 stack **10**. On defining the overlap for the purely translational case, $S(\tau,0) = S(\tau)$, the overlap for the case of translation–rotation symmetry ($\theta \neq 0$) becomes

$$S(\tau,\theta) = S(\tau)\cos(\theta) \ . \tag{17}$$

Thus, for the σ^* orbitals of the H_2 units comprising each H_4 unit of stack **11** we may write

$$S_{ii}(\tau,\theta) = S_{ii}(\tau)\cos(\theta) \quad (i=1,2) \ . \tag{18}$$

The explicit θ-dependence of the off-diagonal matrix elements, $S_{12}(\tau,\theta)$ and $S_{21}(\tau,\theta)$, is best seen by viewing the H_4 stack along the translational axis. Scheme 13 illustrates the view along the translational axis for the H_4 stack **11** – the atom shading from Scheme 11 is retained to enable easy identification of the atoms belonging to the individual H_2 stacks.

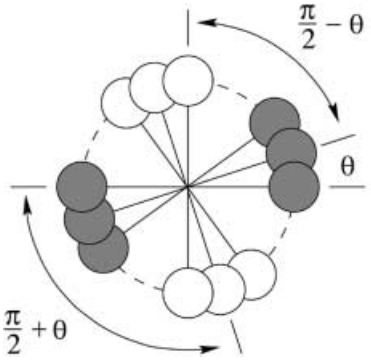

13

The σ^* orbitals associated with the shaded and nonshaded atoms are denoted by the indices 1 and 2, respectively, and the off-diagonal overlaps are written

$$S_{12}(\tau,\theta) = S_{12}(\tau)\cos\left(\frac{\pi}{2}-\theta\right) = S_{12}(\tau)\sin(\theta) \tag{19}$$

and

$$S_{21}(\tau,\theta) = S_{21}(\tau)\cos\left(\frac{\pi}{2}-\theta\right) = -S_{21}(\tau)\sin(\theta) \ . \tag{20}$$

Having extracted the explicit θ-dependence of the matrix $\hat{\mathbf{S}}(\tau,\theta)\mathrm{e}^{ik\tau}$ from Eq. (13) we can now rewrite Eqs. (14), (15), and (16) in terms of the corresponding overlap matrix elements in Eqs. (18), (19), and (20) using the Wolfsberg–Helmholtz relation Eq. (21).

$$H_{\mu\nu} = \frac{\kappa}{2}\left(H_{\mu\mu} + H_{\nu\nu}\right)S_{\mu\nu} = \kappa_{\mu\nu}S_{\mu\nu}, \tag{21}$$

where $S_{\mu\nu} = \langle\phi_\mu|\phi_\nu\rangle$ and $\kappa = 1.75$.

We thus obtain

$$E_i^{(1)}(k,\theta) = \kappa E_1^{(0)}(\theta)S_{ii}(\tau)\cos(\theta)\mathrm{e}^{ik\tau} \quad (i=1,2) \ , \tag{22}$$

$$E_1^{(2)}(k,\theta) = \frac{|\kappa E_1^{(0)}(\theta)S_{12}(\tau)|^2}{\Delta E^{(0)}(\theta)}\sin^2(\theta)\mathrm{e}^{i2k\tau} \ , \tag{23}$$

and

$$E_2^{(2)}(k,\theta) = -\frac{|\kappa E_2^{(0)}(\theta)S_{21}(\tau)|^2}{\Delta E^{(0)}(\theta)}\sin^2(\theta)\mathrm{e}^{i2k\tau} \ . \tag{24}$$

From Eqs. (22), (23), and (24) we are finally able to extract the functional form of the θ- and k-dependence for bands II and III of the H_4 stack.

First consider the case of pure translational symmetry ($\theta = 0$). On substituting expressions for the first- and

second-order corrections to the energy (Eqs. 22, 23, 24) in Eq. (7) we obtain

$$E_1(k,0) \approx E_1^{(0)}(0) + \kappa E_1^{(0)} S_{11}(\tau) e^{ik\tau} \quad , \tag{25}$$

and

$$E_2(k,0) \approx E_2^{(0)}(0) + \kappa E_2^{(0)} S_{22}(\tau) e^{ik\tau} \quad . \tag{26}$$

Since for the case of pure translational symmetry we do not observe a rehybridization of the σ^* basis according to Scheme 12, we can write $E_1^{(0)}(0) = E_2^{(0)}(0)$. Further, by symmetry, the overlap between σ^* orbitals on neighboring H_2 units within the same H_2 stack is the same for both stacks. Thus, we may write $S_{11}(\tau) = S_{22}(\tau)$, and Eqs. (25) and (26) become

$$E_1(k,0) = E_2(k,0) = E_1^{(0)}(0)[1 + \kappa S_{11}(\tau)\cos(k\tau)] \quad . \tag{27}$$

Both the degeneracy of bands II and III for the purely translational case and the "cosine" band topology with respect to the wavevector, k, are accounted for by Eq. (27). The linear relation between the bandwidth [defined by $2E_1^{(0)}(0)\kappa S_{11}(\tau)$ in Eq. 27] and the overlap between σ^* orbitals in neighboring H_4 units, $S_{11}(\tau)$, is in accord with the general assertion that the bandwidth increases with increasing overlap between neighboring structural units in a polymer.

We now consider the transition from pure translational symmetry to translation–rotation symmetry and focus on reproducing the topology of bands II and III for $\theta = \frac{\pi}{6}, \frac{\pi}{4}, \frac{\pi}{3}$ in Fig. 7. In particular, we focus on understanding the progressive distortion of the pure cosine bands for the $\theta = 0$ case that occurs on increasing θ. We note the emergence of increasingly prominent band extrema which, on increasing θ on the interval $0 < \theta < \frac{\pi}{2}$, migrate from the zone edges to the zone center. For the case of θ on the interval $0 < \theta < \frac{\pi}{2}$ both first- and second-order contributions to the band energy, as defined by Eqs. (22), (23), and (24), are nonzero. In order to describe the band topology for $0 < \theta < \frac{\pi}{2}$, we extract the following functional forms from Eq. (7)

$$E_1(k,\theta) \sim E_1^{(0)}(\theta)[\cos(\theta)\cos(k\tau) + \sin^2(\theta)\cos(2k\tau)] \tag{28}$$

and

$$E_2(k,\theta) \sim E_2^{(0)}(\theta)[\cos(\theta)\cos(k\tau) - \sin^2(\theta)\cos(2k\tau)] \tag{29}$$

within the nearest-neighbor approximation.

Equations (28) and (29) are plotted in Fig. 8 for $\theta = \frac{\pi}{6}, \frac{\pi}{4}, \frac{\pi}{3}$ for a constant value of $E_1^{(0)} = E_2^{(0)}$. The plots in Fig. 8 strongly resemble the band topologies given in Fig. 7 for bands II and III of the H_4 stack. As θ increases on the interval $0 < \theta < \frac{\pi}{2}$ we note a gradual reduction in the cosine character of the bands and an increase in the contribution from the $\cos(2k\tau)$ term, which has an extremum at the zone center ($k = \frac{\pi}{2\tau}$). Clearly the emergence of band extrema that do not coincide with either the zone center or the edge is the result of the interactions between the H_2 units of the interpenetrating H_2 chains given by the second-order correction to the band energy.

Compared with the topology of bands II and III, describing the θ- and k-dependence of band IV is relatively straightforward. The analogy between interchain interactions for a pair of interpenetrating H_2 chains and the interactions between bands II and III is not required for the case of the nondegenerate band IV. We need only consider a first-order correction to the energy of the form of Eq. (22), resulting in a band energy function of the form

$$E(k,\theta) = E^{(0)}(\theta)[1 + \kappa S(\tau) e^{ik\tau}] \quad , \tag{30}$$

where the θ-dependence of the zeroth order energy is a result of rehybridization in MO IV and is analogous to Scheme 12 for MOs II and III.

The form of Eq. (30) is the result of considering the topology of band IV to be the result of two noninteracting, interpenetrating H_2 stacks. Thus, the form of the

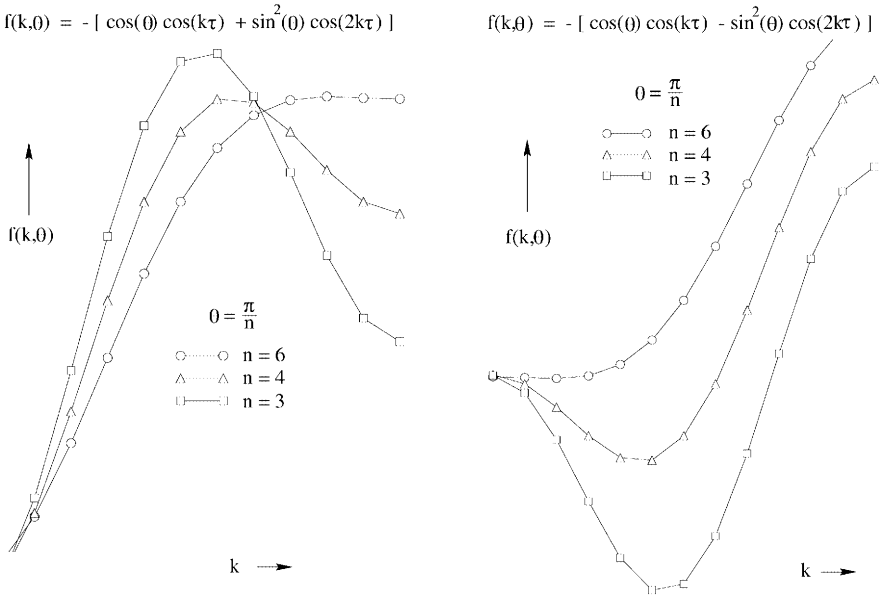

Fig. 8. The functional form of the combined first-and second-order corrections to the band energy of bands II and III of the H_4 stack as a function of the stacking angle and the wavevector, k

first-order correction in Eq. (30) is directly analogous to that for bands II and III.

The $\theta = \frac{\pi}{4}$ case for band IV is equivalent to the $\theta = \frac{\pi}{2}$ case for bands II and III in the sense that it represents an "extremum" in the transition between pure translational symmetry and translation–rotation symmetry. The frequency with which band topologies recur as a function of stacking angle depends on the number of nodal planes posessed by the MOs giving rise to the bands. For instance, the invariance of band I with respect to θ is a direct consequence of the lack of nodal planes in MO I. The symmetry about $\theta = \frac{\pi}{2}$ for bands II and III is a direct consequence of the single nodal plane in MOs II and III and the symmetry about $\theta = \frac{\pi}{4}$ for band IV is a direct result of the two nodal planes posessed by MO IV.

In general, the band resulting from an MO with n nodal planes will exhibit "topological extrema" for

$$\theta_{\max} = \frac{\pi}{2n}; \quad n = 0, 1, 2, \ldots \tag{31}$$

on defining the purely translational case by $\theta = 0$.

The band structure for the H_6 stack as a function of stacking angle, is shown in Fig. 9 and serves to further illustrate this point. The MOs for the H_6 unit are analogous to the π orbitals of benzene and are given in Scheme 14.

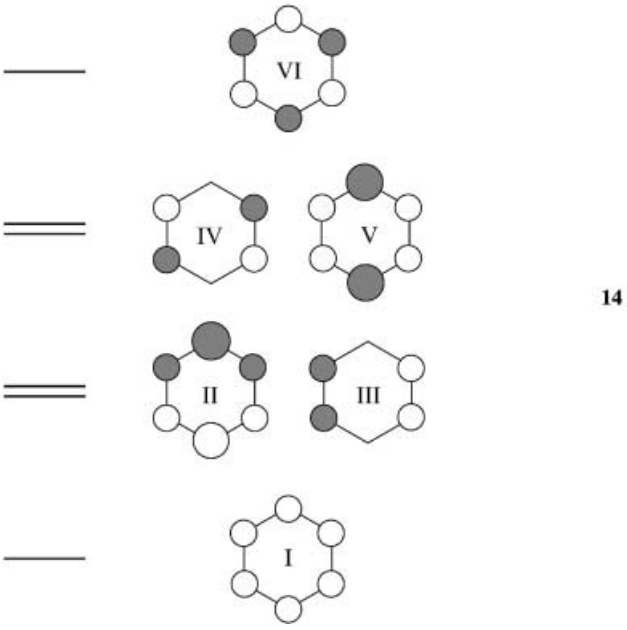

14

The nodeless orbital I is analogous to MO I for H_4; thus, band I for H_6 is also invariant with respect to stacking angle. MOs II and III for H_6 are analogous to MOs II and III for H_4 in the sense that both pairs of MOs exhibit identical phase relationships with respect to their single nodal plane. Similarly, MOs IV and V of H_6 and MO IV of H_4 are asymmetric with respect to both their nodal planes. By analogy with MO IV for H_4 in **9**, MOs IV and V of H_6 can be decomposed into contributions on two orthogonal H_2 units. Thus, on considering the interactions between two interpenetrating H_2 stacks, bands IV and V for H_6 give rise to band structures analogous to those for bands II and III of the H_4 stack.

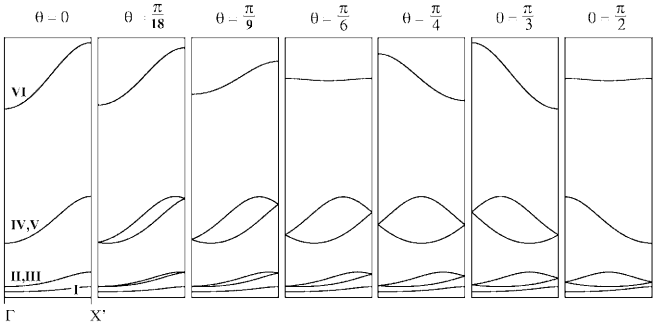

Fig. 9. Band structure of the H_6 stack as a function of the stacking angle

Both pairs of bands (II, III) and (IV, V) for the H_6 stack **14** give rise to band structures with the anticipated "topological extrema" at $\theta_1 = \frac{\pi}{2}$ (one nodal plane) for MOs II and III and $\theta_2 = \frac{\pi}{4}$ (two nodal planes) for MOs IV and V, respectively.

The presence of three nodal planes in MO VI results in a "topological extremum" for band VI at $\theta = \frac{\pi}{6}$, in agreement with the prediction from Eq. (31). The topology of band VI is formally analogous to that of band IV for the H_4 stack and is also described by an expression of the form of Eq. (30).

The topology of bands IV and VI of the H_4 and H_6 stacks, respectively, are noteworthy in that the band shapes at the topological extrema cannot be described without extending our theoretical framework. The topology of band IV for $\theta = \frac{\pi}{4}$ is identical to the topology of the σ^* band of the alternating H_2 stack shown in Fig. 6. The "energy oscillation" on tracing out the path $a \rightarrow b \rightarrow c$ in Fig. 6 is the result of differences in interaction between next-nearest-neighbor H_2 units of the stack. The same is true for band VI of the H_4 stack and band VI of the H_6 stack. Since the interaction between next-nearest-neighbor units in these polymers result in bandwidths at least an order of magnitude less than the first-order corrections (Eq. 30), we choose to retain our focus on nearest-neighbor interactions and simply note the origins of these minor energy perturbations.

We conclude this discussion of band topology by examining the similarities and differences between JZ and BZ representations of band structure for translational cells equivalent to one complete turn of the helix. As noted for the H_2 stack, such representations can be mapped onto one another and we concluded that the JZ representation was equivalent to the BZ representation for a doubled translational cell. We now investigate such mappings for a more general class of polymers with translation–rotation symmetry. Consider a polymer with translation–rotation symmetry and a stacking angle $\theta = \frac{2\pi}{n}$, where n is the number of structural units per turn of the helix. The JZ can be mapped onto an "extended BZ" consisting of the first n BZs according to

$$[\Gamma, X'] \longrightarrow [\Gamma, nX] \ . \tag{32}$$

The band structures for H_3 and H_4 stacks defined by $n = 3$ and $n = 4$, respectively, are shown in Figs. 10 and 11 respectively in both the JZ and the extended BZ representations.

The mapping between the extended BZ and JZ representations might at first seem improbable given the possible existence of band extrema that do not coincide with either the zone center or the edges in the JZ representation; however, on superimposing the band structures for the H_3 and H_4 stacks in the JZ representation on the extended BZ defined by Eq. (32) we note that the band extrema in the JZ representation coincide with the boundaries between the individual BZs contained within the extended BZ. If we subsequently apply the translational symmetry of the helix (which corresponds to translations by $2X = \frac{2\pi}{a}$ in the extended BZ) to the JZ representation we are able to map the band structure in the JZ representation onto the extended BZ band structure. Indeed by applying translational symmetry to the band extrema in the JZ representation we are able to map all extrema to extrema at the center or edge of the first BZ. Thus, we can now understand the equivalence of band structures based on the JZ and extended BZ representations for translational cells corresponding to a complete turn of the helix.

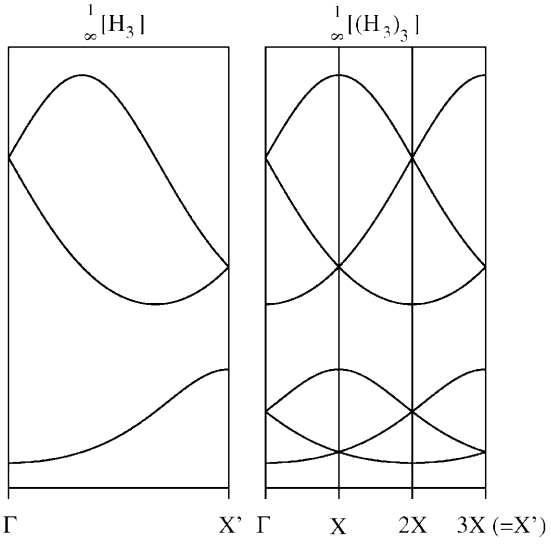

Fig. 10. Band structure for the H_3 stack with three units per translational cell in the JZ (*left*) and extended BZ (*right*) representations

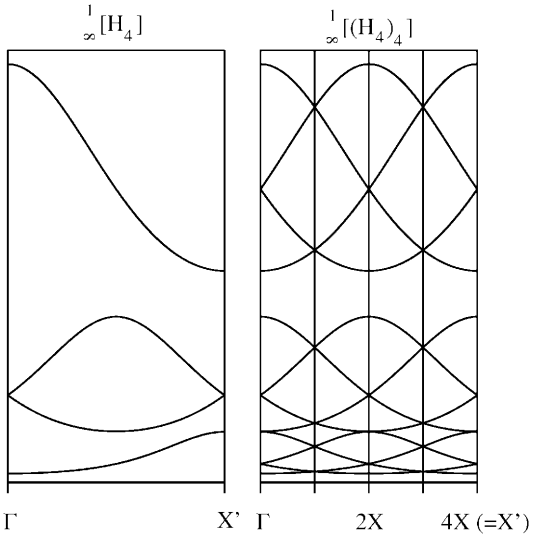

Fig. 11. Band structure for the H_4 stack with four units per translational cell in the the JZ (*left*) and extended BZ (*right*) representation

6 Conclusion

In this contribution we have investigated the effect of varying the size of the translational repeat unit and the structure of the chemical repeat unit on the band structure of quasi-one-dimensional polymers posessing helical (screw-axis) symmetry.

We have demonstrated the equivalence of band structure representations based on translation–rotation symmetry (JZ representation) and pure translational symmetry for the specific case of a translational cell equivalent to a complete turn of the helix generated by the intrinsic translation–rotation symmetry. Thus, when evaluating the physical properties of polymers with translation–rotation symmetry it is necessary to sample either the JZ ($\Gamma \rightarrow X'$) or the BZ ($\Gamma \rightarrow X$) on constructing the polymer from a translational cell equivalent to a complete turn of the helix.

We hope that our perturbative treatment of orbital interactions in polymers with translation–rotation symmetry will serve as a general model which can be subsequently employed in the design of polymers with specific electronic properties.

Appendix

The calculations were performed with a modified version of the program Bind, which is available as part of the YAeHMOP extended Hückel package [7]. The extended Hückel parameters for hydrogen ($H_{1s} = -13.6$ eV, $\zeta_{1s} = 1.300$) were taken from previous studies by our group.

An H–H bond length of 0.8 Å and an H_2–H_2 separation of 1.1 Å were used to construct the H_2 stacks. The H_3, H_4, and H_6 stacks were constructed using an H–H bond length of 1.0 Å and a separation of 1.2 Å between adjacent structural units in the stacks.

References

1. Bozovic I (1984) Phys Rev B 29: 6586
2. Landrum GA (1997) Ph D dissertation. Cornell University
3. Blumen A, Merkel C (1977) Phys Stat Sol B 83: 425
4. Elliott S (1998) The physics and chemistry of solids. Wiley, New York
5. Kollmar C, Hoffmann R (1990) J Am Chem Soc 112: 8230
6. Hoffmann R, Janiak C, Kollmar C (1991) Macromolecules 24: 3725
7. http://www.sourceforge.net/projects/yaehmop/